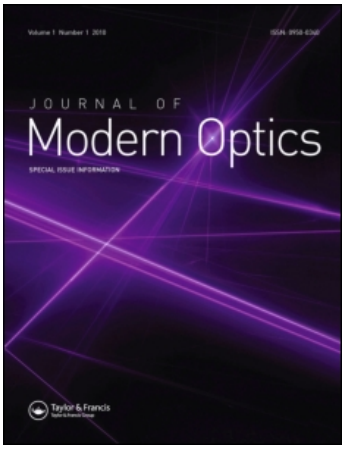

Journal of Modern Optics
Publication details, including instructions for authors and subscription information:
http://www.informaworld.com/smpp/title~content=t713191304

Recent progress in third generation infrared detectors

A. Rogalski[a]
[a] Institute of Applied Physics, Military University of Technology, 00-908 Warsaw, Poland

First published on: 25 June 2010

To cite this Article Rogalski, A.(2010) 'Recent progress in third generation infrared detectors', Journal of Modern Optics, 57: 18, 1716 — 1730, First published on: 25 June 2010 (iFirst)
To link to this Article: DOI: 10.1080/09500340.2010.486485
URL: http://dx.doi.org/10.1080/09500340.2010.486485

Journal of Modern Optics
Vol. 57, No. 18, 20 October 2010, 1716–1730

Taylor & Francis
Taylor & Francis Group

Recent progress in third generation infrared detectors

A. Rogalski*

Institute of Applied Physics, Military University of Technology, 2 Kaliskiego Str., 00-908 Warsaw, Poland

(*Received 12 January 2010; final version received 25 March 2010*)

In this paper, issues associated with the recent development third generation detectors are discussed. In this class of detectors HgCdTe photodiodes, type II superlattice photodiodes, quantum-well infrared photoconductors (QWIPs), and quantum dot IR photodetectors (QDIPs) are considered. The main challenges facing multicolor devices concern complicated device structures, thicker and multilayer material growth, and more difficult device fabrication, especially when the array size gets larger and pixel size gets smaller. Also discussion on the on-going detector technology efforts is presented.

Keywords: third generation infrared detectors; HgCdTe photodiodes; InAs/GaSb superlattice photodiodes; QWIPs; QDIPs

1. Introduction

Multispectral infrared (IR) focal plane arrays (FPAs) are highly beneficial for a variety of applications such as missile warning and guidance, precision strike, overhead surveillance, target detection, recognition, acquisition and tracking, thermal imaging, navigational aids and night vision, etc. They can also play many important roles in Earth and planetary remote sensing and astronomy. Systems that gather data in separate IR spectral bands can discriminate both absolute temperature and unique signatures of objects in the scene [1]. By providing this new dimension of contrast, multiband detection also offers advanced color processing algorithms to further improve sensitivity above that of single-color devices. This is extremely important for identifying temperature differences between missile targets, warheads, and decoys.

In the 1990s third generation IR detectors emerged after the tremendous impetus provided by detector developments. The definition of third generation IR systems is not particularly well established. In the common understanding, third generation IR systems provide enhanced capabilities such as larger number of pixels, higher frame rates, better thermal resolution, as well as multicolor functionality and other on-chip signal processing functions. According to Reago et al. [2], the third generation is defined by the requirement to maintain the current advantage enjoyed by the U.S. and allied armed forces. This class of devices includes both cooled and uncooled FPAs [2,3]:

- high performance, high resolution cooled imagers having multi-color bands,
- medium to high performance uncooled imagers,
- very low cost, expendable uncooled imagers.

When developing third generation imagers, the IR community is faced with many challenges. Current readout technology is based upon CMOS circuitry that has benefited from dramatic and continuing progress in miniaturizing circuit dimensions. Second generation imagers provide *NEDT* of about 20–30 mK with $f/2$ optics. A goal of third-generation imagers is to achieve sensitivity improvement corresponding to *NEDT* of about 1 mK. In a 300 K scene in the LWIR region with thermal contrast of 0.02, the required charge storage capacity is above 10^{-9} electrons. This high charge-storage density cannot be obtained within the small pixel dimensions using standard CMOS capacitors [3].

To provide an opportunity to significantly increase both the charge storage capacity and the dynamic range, the vertically-integrated sensor array (VISA) program has been sponsored by DARPA [4–6]. The approach being developed builds on the traditional 'hybrid' structure of a detector with a 2D array of indium-bump interconnects to the silicon readout. VISA allows additional layers of silicon processing chips to be connected below the readout to provide more complex functionality. It will allow the use of

*Email: rogan@wat.edu.pl

ISSN 0950–0340 print/ISSN 1362–3044 online

DOI: 10.1080/09500340.2010.486485
http://www.informaworld.com

smaller and multicolor detectors without compromising storage capacity. Signal-to-noise ratios will increase for multicolor focal plane arrays. This will permit LWIR focal plane arrays to improve the sensitivity by a factor of 10.

Pixel and chip sizes are important issues in association with multi-color imager formats. Small pixels reduce cost by increasing the number of readout and detector dice potentially available from processed wafers. Small pixels also allow smaller, lightweight optics to be used.

Recently, the first large format MWIR FPAs with pixel dimension of 15 μm have been demonstrated [7,8]. It will be an extreme challenge to deploy a two- or three-color detector structure into a small pixel such as $18 \times 18\,\mu m^2$. Current two-color simultaneous mode pixels with two indium bumps per pixel have not been built with pixels smaller than 25 μm on a side.

In the IR regions of interest such as short wavelength IR (SWI, middle wavelength IR (MWIR) and long wavelength IR (LWIR), four detector technologies present multicolor capability: HgCdTe photodiodes, quantum well infrared photodetectors (QWIPs), antimonide based type II strained-layer superlattice (SLS) photodiodes, and quantum dot infrared photodetectors (QDIPs) [1]. In this paper, recent progress in third generation IR is presented.

2. Dual-band HgCdTe detectors

The standard method to detect multiwavelength simultaneously is to use optical components such as lenses, prisms and gratings to separate the wavelength components before they impinge on the IR detectors. Another simpler method is a stacked arrangement in which the shorter wavelength detector is placed optically ahead of the longer wavelength detector. In such a way, two-color detectors using HgCdTe [9] and InSb/PbSnTe [10] photodetectors were demonstrated in the early 1970s. At present, however, considerable efforts are directed to fabricating a single FPA with multicolor capability to eliminate the spatial alignment and temporal registration problems that exist whenever separate arrays are used, to simplify optical design, and to reduce size, weight, and power consumption.

The unit cell of integrated multi-color FPAs consists of several co-located detectors, each sensitive to a different spectral band (see Figure 1). Radiation is incident on the shorter band detector, with the longer wave radiation passing through to the next detector. Each layer absorbs radiation up to its cutoff, and hence transparent to the longer wavelengths, which are then collected in subsequent layers. In the case of HgCdTe, this device architecture is realized by placing a longer wavelength HgCdTe photodiode optically behind a shorter wavelength photodiode.

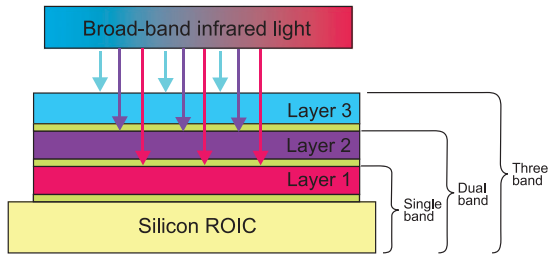

Figure 1. Structure of a three-color detector pixel. Infrared flux from the first band is absorbed in Layer 3, while longer wavelength flux is transmitted through the next layers. The thin barriers separate the absorbing bands. (The color version of this figure is included in the online version of the journal.)

Back-to-back photodiode two-color detectors were first implemented using quaternary III–V alloy ($Ga_xIn_{1-x}As_yP_{1-y}$) absorbing layers in a lattice matched InP structure sensitive to two different SWIR bands [11]. A variation on the original back-to-back concept was implemented using HgCdTe at Rockwell [12] and Santa Barbara Research Center [13]. Following the successful demonstration of multispectral detectors in LPE-grown HgCdTe devices [13], the MBE and MOCVD techniques have been used for the growth of a variety of multispectral detectors at Raytheon [14–20], BAE Systems [21], Leti [22–27] Selex and QinetiQ [28–31], DRS [32–34] Teledyne and NVESD [35,36]. For more than a decade steady progression has been made in a wide variety of pixel sizes (to as small as 20 μm), array formats (up to 1280×720) and spectral-band sensitivity (MWIR/MWIR, MWIR/LWIR and LWIR/LWIR).

Both sequential mode and simultaneous mode detectors are fabricated from multilayer materials. The simplest two-color HgCdTe detector, and the first to be demonstrated, was the bias-selectable n-P-N triple-layer heterojunction (TLHJ), back-to-back photodiode shown in Figure 2(*a*) (capital letter means wider band gap structure). The n-type base absorbing regions are deliberately doped with indium at a level of about $(1 \text{ to } 3) \times 10^{15}\,cm^{-3}$. A critical step in device formation is ensuring that the *in situ* p-type As-doped layer (typically 1–2 μm thick) has good structural and electrical properties to prevent internal gain from generating spectral crosstalk. The band gap engineering effort consists of increasing the CdTe mole fraction and the effective thickness of the p-type layer to keep out-of-band carriers from being collected at the terminal.

The sequential-mode detector has a single indium bump per unit cell that permits sequential bias

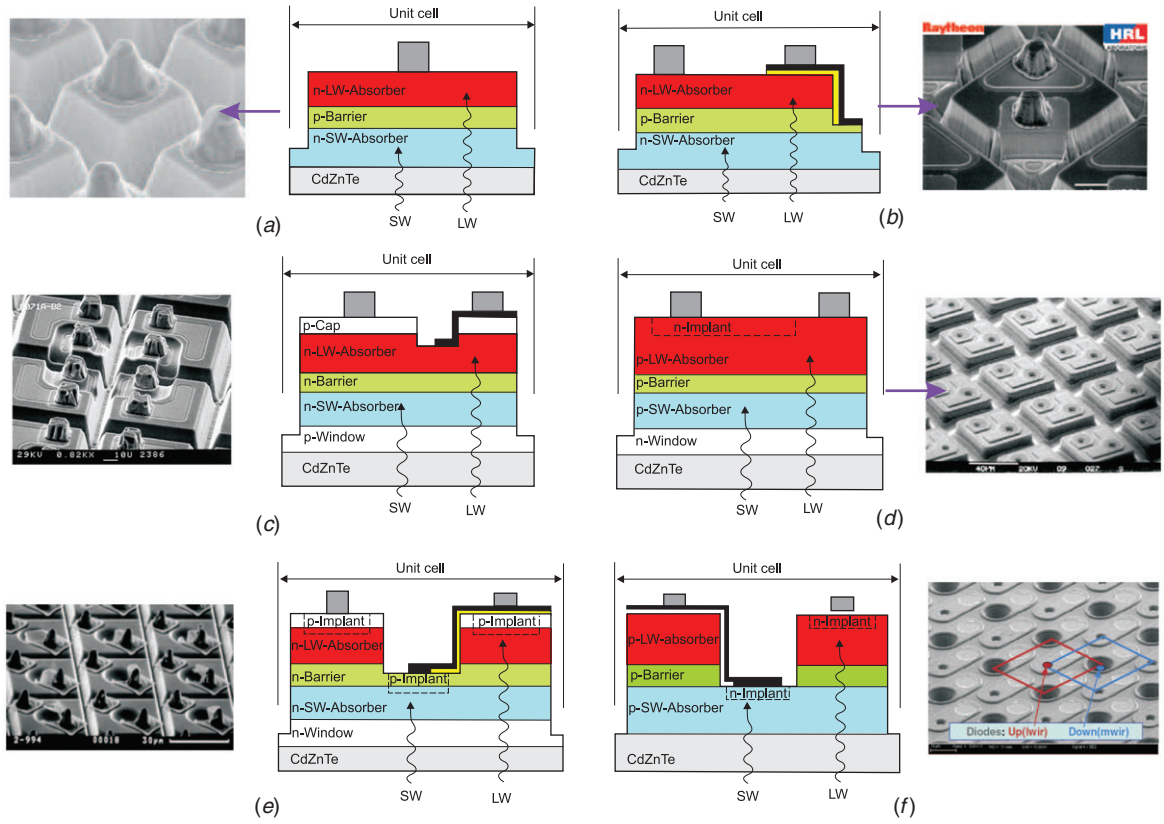

Figure 2. Cross-section views of unit cells for various back-illuminated dual-band HgCdTe detector approaches: (*a*) bias-selectable n-p-n structure reported by Raytheon [13], (*b*) simultaneous n-p-n design reported by Raytheon [14], (*c*) simultaneous p-n-n-p reported by BAE Systems [21], (*d*) simultaneous n-p-p-p-n design reported by Leti [22], (*e*) simultaneous structure based on p-on-n junctions reported by Rockwell [35], and (*f*) simultaneous structure based on n-on-p junctions reported by Leti [26]. (The color version of this figure is included in the online version of the journal.)

selectivity of the spectral bands associated with operating back-to-back photodiodes. When the polarity of the bias voltage applied to the bump contact is positive, the top (LW) photodiode is reverse biased and the bottom (SW) photodiode is forward biased. The SW photocurrent is shunted by the low impedance of the forward-biased SW photodiode, and the only photocurrent to emerge in the external circuit is the LW photocurrent. When the bias voltage polarity is reversed, the situation reverses; only the SW photocurrent is available. Switching times within the detector can be relatively short, on the order of microseconds, so detection of slowly changing targets or images can be achieved by switching rapidly between the MW and LW modes. The problems with the bias-selectable device are the following: its construction does not allow independent selection of the optimum bias voltage for each photodiode, and there can be substantial MW crosstalk in the LW detector.

Multicolor detectors require deep isolation trenches to cut completely through the relatively thick (at least 10 μm) LWIR absorbing layer. The design of small two-color TLHJ detectors of less than 20 μm pitch requires at least 15 μm deep trenches, which are no more than 5 μm wide at the top. Dry etching technology has been used for a number of years to produce two-color detectors. One of the materials technologies being developed in order to meet the challenge of shrinking the pixel size to below 20 μm is advanced etching technology. Recently, Raytheon has developed an inductively coupled plasma (ICP) dry mesa etching capability to replace electron cyclotron resonance (ECR) dry mesa etching. The ICP, when compared to ECR, has shown reduced lateral mask erosion during etching, less significant etch-lag effects, and improved etch depth uniformity [37]. For the pseudo-planar devices the etching step is easier to perform because of the lower aspect ratio. Moreover, there is no electrical crosstalk as the pixels are electrically independent.

Many applications require true simultaneous detection in the two spectral bands. This has been achieved in a number of ingenious architectures shown in Figure 2(*b*)–(*f*). Two different architectures are shown.

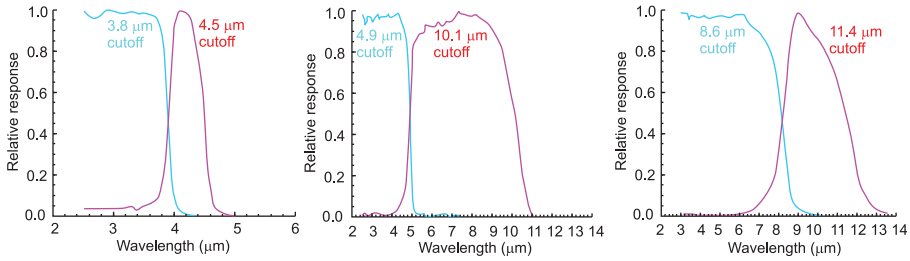

Figure 3. Spectral response curves for two-color HgCdTe detectors in various dual-band combinations of MWIR and LWIR spectral bands (after [39]). (The color version of this figure is included in the online version of the journal.)

The first one is the classical n-P-N back-to-back photodiode structure (Figure 2(*b*)). In the case of the architecture developed at Leti (Figure 2(*d*)), the two absorption materials are p-type separated by a barrier to prevent any carrier drift between the two n-on-p diodes. Each pixel consists of two standard n-on-p photodiodes, where the p-type layers are usually doped with Hg vacancies. The shorter wavelength diode is realized during epitaxy by simply doping part of the first absorbing layer with In. The longer wavelength junction is obtained by a planar implantation process. It should be noted that the electron mobility is around 100 times greater in n-type material than holes in p-type material and, hence, the n-on-p structures will have a much lower common resistance. This is an important consideration for large area FPAs with detection in the LW range due to the larger incident-photon flux.

The last two architectures shown in Figure 2(*e*) and (*f*), called 'pseudo-planar', present a totally different approach. They are close to the structure proposed by Lockwood et al. [38] in 1976 for PbTe/PbSnTe heterostructure two-color photodiodes. They are based on the concept of two p-on-n (Figure 2(*e*)) or n-on-p (Figure 2(*f*)) diodes fabricated by p-type or n-type implantation, respectively, but on two different levels of a three-layer heterostructure. The architecture developed by Rockwell is a simultaneous two-color MWIR/LWIR FPA technology based on a double-layer planar heterostructure (DLPH) MBE technology (Figure 2(*e*)). To prevent the diffusion of carriers between two bands, a wide-band gap 1 μm thick layer separates these two absorbing layers. The diodes are formed by implanting arsenic as a p-type dopant and activating it with an anneal. This results in a unipolar operation for both bands. The implanted area of Band 2 is a concentric ring around the Band 1 dimple. Because the lateral carrier-diffusion length is larger than the pixel pitch in the MWIR material, and the Band 1 junction is shallow, each pixel is isolated by dry-etching a trench around it to reduce carrier crosstalk. The entire structure is capped with a layer of material with a slightly wider band gap to reduce surface recombination and simplify passivation.

All these simultaneous dual-band detector architectures require an additional electrical contact from an underlying layer in the multijunction structure to both the SW and the LW photodiode. The most important distinction is the requirement of a second readout circuit in each unit cell.

It is expected that with the TLHJ architecture, pixel size could decrease to 15 μm, and array format could increase to several megapixels. With the pseudo-planar architecture, MWIR/LWIR devices should be produced more easily, with large format arrays having pixel size around 20 μm.

Figure 3 illustrates examples of the spectral response from different two-color devices. Note that there is minimal crosstalk between the bands, since the short-wavelength detector absorbs nearly 100% of the shorter wavelengths. Test structures indicate that the separate photodiodes in a two-color detector perform exactly like single-color detectors in terms of achievable R_0A variation with wavelength at a given temperature.

The best performing bias selectable dual-color FPAs being produced at Reytheon Vision Systems exhibit out-of-band crosstalk below 10%, 99.9% interconnect operability, and 99% response operability which is comparable to state-of-the-art, single-color technology. It is predicted that ongoing development of material growth and fabrication processes will translate to further improvements in dual-color FPA performance.

Recently, Raytheon Vision Systems has developed two-color, large-format infrared FPAs to support the US Army's third generation FLIR systems in both 640×480) and 'high-definition' 1280×720 formats with 20×20 μm unit cells (see Figure 4). The ROICs share a common chip architecture and incorporate identical unit cell circuit designs and layouts; both FPAs can operate in either dual-band or single-band modes. High-quality MWIR/LWIR 1280×720 FPAs with cutoffs ranging out to 11 μm at 78 K have

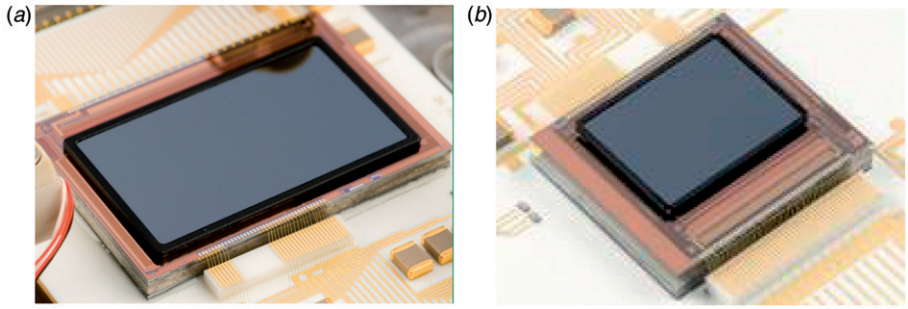

Figure 4. RVS dual-band MW/LWIR FPAs mounted on dewar platforms: (*a*) 1280 × 720 format and (*b*) 640 × 480 format (after [19]). (The color version of this figure is included in the online version of the journal.)

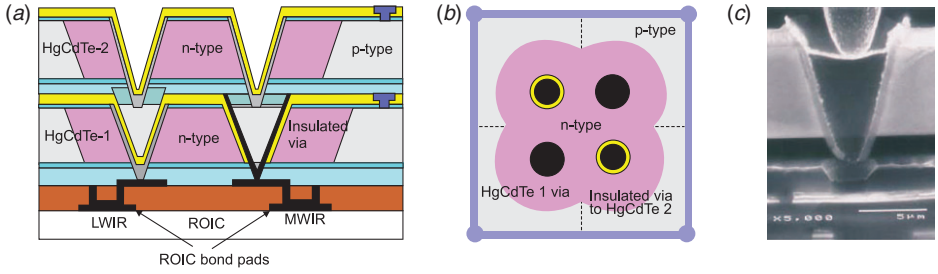

Figure 5. Two-color HDVIP architecture is composed to two layers of thinned HgCdTe epoxied to a silicon readout: (*a*) side view, (*b*) top view (after [34]), and (*c*) small hole etched to form junction and to contact the Si readout. (The color version of this figure is included in the online version of the journal.)

demonstrated excellent sensitivity and pixel operabilities exceeding 99.9% in the MW band and greater than 98% in the LW band. Median 300 K *NEDT* values at *f*/3.5 of approximately 20 mK for the MW and 25 mK for the LW have been measured for dual-band time division multiplexed integration (TDMI) operation at 60 Hz frame rate with integration times corresponding to roughly 40% (MW) and 60% (LW) of full well charge capacities. Excellent high resolution IR camera imaging with *f*/2.8 FOV broadband refractive optics at 60 Hz frame rate has been achieved.

The HgCdTe high-density vertically integrated photodiode (HDVIP) or loophole concept, developed at DRS and BAE Southampton, represents an alternative approach to IR FPA architecture. It differs from the more entrenched FPA architectures in both its method of diode formation and the manner of its hybridization to the silicon ROIC [34]. The monocolor HDVIP architecture consists of a single HgCdTe epilayer grown on CdZnTe substrate by LPE or MBE. After epitaxial growth, the substrate is removed and the HgCdTe layer is passivated on both surfaces with interdiffused layers of evaporated CdTe (the interdiffusion at 250°C on the Te-rich side of the phase field generates about $10^{16}\,\mathrm{cm}^{-3}$ metal vacancies). During this process the Cu can also be in-diffused from a doped ZnS source providing an alternative to doping during growth. This single color architecture has been extended to two colors at DRS by gluing two monocolor layers together into a composite, and forming an insulated via through the lower layer in order to read out the upper color, as illustrated in Figure 5. Contact to the Si ROIC is obtained by etching holes (or vias) through the HgCdTe down to contact pads on the Si (see Figure 5(*c*)). The ROIC used for the dual-band FPA was originally designed for a single-color 640 × 480 array with 25 μm (square) pixels. The even-numbered rows of the ROIC have no detectors attached to them, so the chip is operated in a mode that only outputs the odd rows. Odd-numbered columns connect to LWIR detectors, and the MWIR detectors are on the even columns. This approach has been utilized to fabricate both MW-LW and MW-MW 240 × 320 FPAs on a 50 μm pitch. Higher densities are being investigated with dedicated two-color ROIC designs, enabling pitches of <30 μm for two-color FPAs.

It is well known that, when the detectivity is approaching a value above $10^{10}\,\mathrm{cm\,Hz^{1/2}\,W^{-1}}$, the FPA performance is uniformity limited prior to correction and thus essentially independent of the detectivity. For short wavelength IR (≈3 μm) and

MWIR (≈5 μm) HgCdTe materials, the variation in cut-off wavelength is not large. However, the non-uniformity is a serious problem in the case of LWIR HgCdTe detectors. The variation of x across the $Hg_{1-x}Cd_xTe$ wafer causes much larger spectral non-uniformity. At 77 K, a variation of $\Delta x = 0.1\%$ gives a $\Delta\lambda_c$ above 0.5 μm at $\lambda_c = 20$ μm, which cannot be corrected by either two or three point corrections. This cut-off wavelength nonuniformity at the FPA level can be spectrally corrected by using a cold filter, but the dark current variation caused by the variation of cutoff wavelengths will still exist. For applications that require operation in the LWIR band as well as two-color LWIR/VLWIR bands, most probably HgCdTe will not be the optimal solution.

An alternative candidate for third generation IR detectors is the Sb-based III–V material system. These materials are mechanically robust and have fairly weak dependence of the band gap on composition (see Figure 6). One advantage of using type II superlattice in LW and VLWIR is the ability to fix one component of the material and vary the other to tune wavelength (see Figure 7).

3. Type-II InAs/GaInSb dual-band detectors

Recently, type II InAs/GaInSb strained-layer superlattices (SLSs) have emerged as a third candidate for third generation infrared detectors [41–46]. Sensors for the MWIR and LWIR spectral ranges are based on binary InAs/GaSb short-period superlattices. The layers needed are already so thin that there is no benefit to using GaInSb alloys.

The type-II superlattice has staggered band alignment such that the conduction band of the InAs layer is lower than the valence band of the InGaSb layer. This creates a situation in which the energy band gap of the superlattice can be adjusted to form either a semi-metal (for wide InAs and GaInSb layers) or a narrow band gap (for narrow layers) semiconductor material. In the SL, the electrons are mainly located in the InAs layers, whereas holes are confined to the GaInSb layers, which suppresses Auger recombination mechanisms and thereby enhances carrier lifetime. The band gap of the SL is determined by the energy difference between the electron miniband and the first heavy hole state at the Brillouin zone center. As is described in [8], the $InAs/Ga_{1-x}In_xSb$ SLSs material system can have some advantages over bulk HgCdTe.

InAs/GaInSb SL photodiodes are typically based on p-i-n structures with an unintentionally doped, intrinsic region between the heavily doped contact portions of the device. A cross-section scheme of a completely processed mesa detector is presented in Figure 8. The layers are usually grown by MBE at

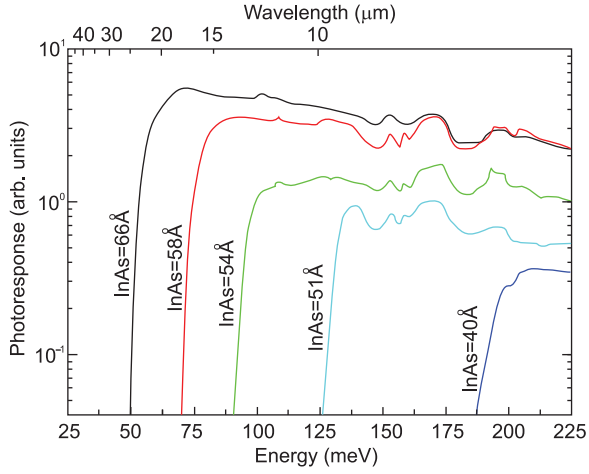

Figure 7. Dependence of the SLS cut-off wavelength with the InAs thickness while GaSb is fixed at 40 angstroms (after [40]). (The color version of this figure is included in the online version of the journal.)

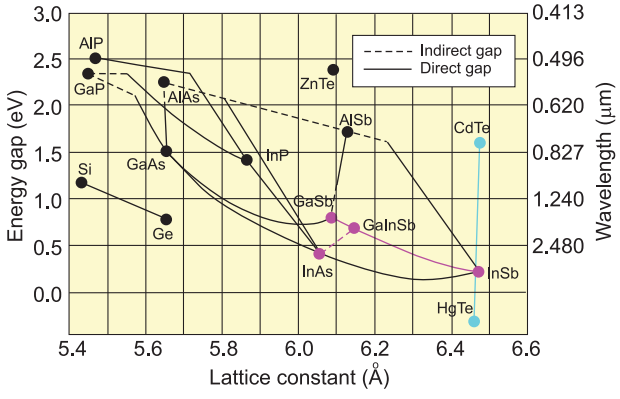

Figure 6. The low temperature energy band gap of semiconductors versus their lattice constants. (The color version of this figure is included in the online version of the journal.)

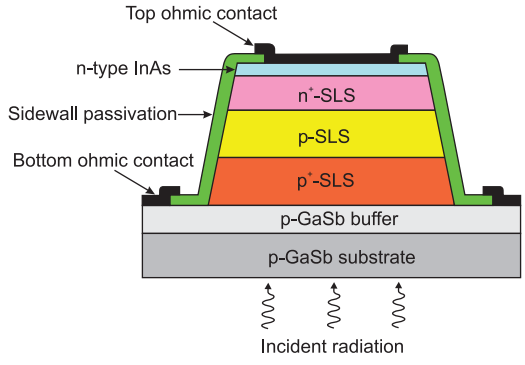

Figure 8. Cross-section schematic of p-i-n InAs/GaSb superlattice photodiode. (The color version of this figure is included in the online version of the journal.)

substrate temperatures around 400°C on undoped (001) oriented two-inch GaSb substrates. With the addition of cracker cells for the group V sources, the superlattice quality becomes significantly improved. The lower periods of the SLs are p-doped with $1 \times 10^{17}\,cm^{-3}$ Be in the GaSb layers. These acceptor doped SL layers are followed by a 1 to 2 μm thick, nominally undoped, superlattice region. The width of the intrinsic region does vary in the designs. The width used should be correlated to the carrier diffusion lengths for improved performance. The upper of the SL stack is doped with silicon (1×10^{17} to $1 \times 10^{18}\,cm^{-3}$) in the InAs layers and is typically 0.5 μm thick. The top of the SL stack is then capped with an InAs:Si ($n \approx 10^{18}\,cm^{-3}$) layer to provide good ohmic contact.

The main technological challenge for the fabrication of photodiodes is the growth of thick SLS structures without degrading the materials quality. High-quality SLS materials thick enough to achieve acceptable quantum efficiency is crucial to the success of the technology. Surface passivation is also a serious problem. Considerable surface leakage is attributed to the discontinuity in the periodic crystal structure caused by mesa delineation. Several materials and processes have been explored for device passivation. Some of the more prominent thin films studied have been silicon nitride, silicon oxides, ammonium sulfide, and aluminium gallium antimonide alloys. The best results have been recently obtained using inductively coupled plasma dry etching and polyimide passivation [46].

The growth sequence of high quality two-color MWIR type-II SLS FPAs fabricated at the Fraunhofer Institute in Freiburg starts with a 200 nm lattice matched AlGaAsSb buffer layer followed by a 700 nm thick n-type doped GaSb layer. Next, the 'blue channel' consisting of 330 periods of p-type of a 7.5 ML InAs/10 ML GaSb is deposited. After the 'blue channel' follows a common ground contact layer comprising 500 nm of p-type GaSb follows. The detection of the 'red channel' is realized using 150 periods of a 9.5 ML InAs/10 ML GaSb superlattice. Finally, 20 nm thick InAs layer terminates the structure. The thickness of the entire vertical pixel structure is only 4.5 μm, which significantly reduces the technological challenge in comparison to dual-band HgCdTe FPAs with a typical total layer thickness around 15 μm.

The first dual-band 288×384 MWIR InAs/GaSb camera has already been demonstrated [42]. Figure 9 illustrates the device processing. In the first step via holes to the common p-type contact layer and to the n-type contact layer of the lower diode are etched by chlorine-based chemically assisted ion beam etching. Next, another chemical etching is used to fabricate

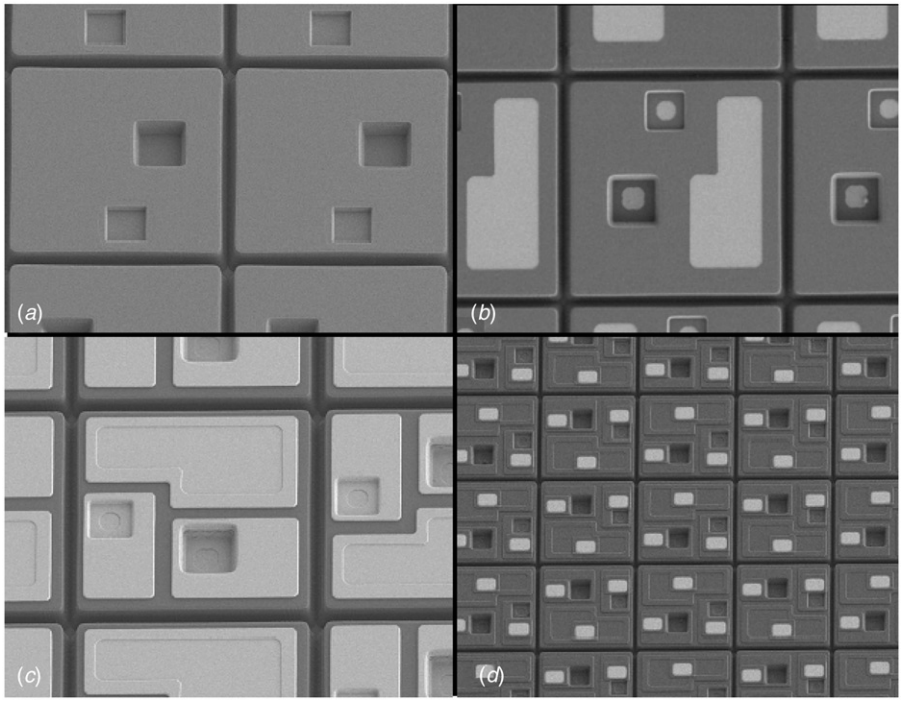

Figure 9. SEM images illustrating the processing of 288 × 384 dual-color InAs/GaSb SLS FPAs. At a pixel pitch of 40 μm, three contact lands per pixel permit simultaneous and spatially coincident detection of both colors (after [42]).

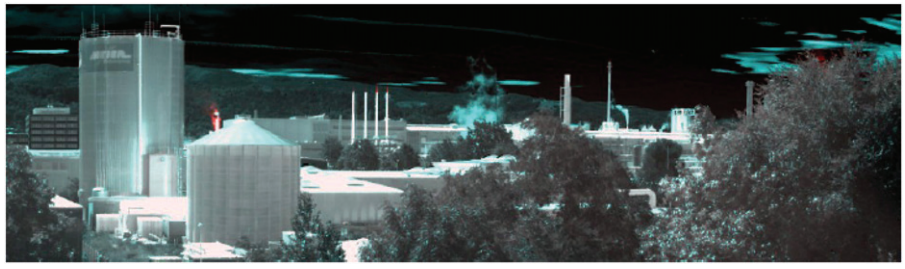

Figure 10. Bispectral infrared image of an industrial site taken with a 384 × 288 dual-color InAs/GaSb SL camera. The two color channels 3–4 μm and 4–5 μm are represented by the complementary colors cyan and red, respectively (after [45]). (The color version of this figure is included in the online version of the journal.)

deep trenches for complete electrical isolation of each pixel (see Figure 9(*a*)). After deposition of the diode passivation, a reactive ion etching is employed to selectively open the passivation to provide access to the contact layers (see Figure 9(*b*)). Next, the contact metallization is evaporated (see Figure 9(*c*)). A fully processed dual-color FPA is shown in Figure 9(*d*).

In the above approach, simultaneous detection in a 40 μm pixel has been achieved. With *f*/2 optics, 2.8 ms integration time and 73 K detector temperature, the superlattice camera achieves an *NEDT* of 29.5 mK for the blue channel ($3.4\,\mu m \leq \lambda \leq 4.1\,\mu m$) and 16.5 mK for the red channel ($4.1\,\mu m \leq \lambda \leq 5.1\,\mu m$). As an example, the excellent imagery delivered by the 288×384 InAs/GaSb dual-color camera is presented in Figure 10. The image is a superposition of the images of the two channels coded in the complimentary colors cyan and red for the detection ranges of 3–4 μm and 4–5 μm, respectively. The red signatures reveal hot CO_2 emissions in the scene, whereas water vapor, e.g. from steam exhausts or in clouds, appear blue due to the frequency dependency of the Rayleigh scattering coefficient.

As one of the first representatives of a third generation system, the dual-color SLS technology is commercialized in a missile approach warning system [44]. These very promising results confirm that the antimonide SL technology is now a direct competitor to MBE HgCdTe dual-color technology.

4. Multiband QWIPs

QWIPs are ideal detectors for the fabrication of pixel co-registered simultaneously readable two-color IR FPAs because a QWIP absorbs IR radiation only in a narrow spectral band and is transparent outside of that absorption band. Thus, it provides zero spectral crosstalk when two spectral bands are more than a few microns apart. Individual pixels in a multiband QWIP detector array are fabricated using a process similar to that used for their single band counterparts, except for the via holes that need to be added to electrically connect with the silicon ROIC.

Sanders was the first organization to fabricate two-color, 256 × 256 bound-to-miniband QWIP FPAs in each of four important combinations: LWIR/LWIR, MWIR/LWIR, near-IR (NIR)/LWIR, and MWIR/MWIR – with simultaneous integration [47,48]. At present multicolor QWIP detectors are fabricated at Jet Propulsion Laboratory (JPL) [49–55], Army Research Laboratory [56–58], Goddard [58,59], Thales [60–64], and AIM [42,65,66] with the majority being based on bound-to-extended transitions.

Devices capable of simultaneously detecting two separate wavelengths can be fabricated by vertical stacking of the different QWIP layers during epitaxial growth. The long-wavelength-sensitive stack (red QWIP) is grown above the shorter-wavelength-sensitive stack (blue QWIP). As shown in Figure 11(*b*), the carriers emitted from each multi-quantum well (MQW) region are collected separately using three contacts. The middle contact layer (see Figure 11(*c*)) is used as the detector common. The electrical connections to the detector common and the LWIR connection are brought to the top of each pixel using via connections. Electrical connections to the common contact and the LWIR pixel connection are brought to the top of each pixel using the gold via connections visible in Figure 11(*d*). This elaborate processing technology could lead to 2D imaging arrays that can detect three separate bands on a single pixel.

The gaps between FPA detectors and the readout multiplexer are backfilled with epoxy. The epoxy backfilling provides the necessary mechanical strength to the detector array and readout hybrid prior to array thinning. The initial GaAs substrate of dual-band FPAs is completely removed leaving only a 50 nm thick GaAs membrane. This allows the array to accommodate any thermal expansion by eliminating the thermal mismatch between the silicon readout and the detector array. It also eliminates pixel-to-pixel crosstalk and, finally, significantly enhances the optical coupling of IR radiation into the QWIP pixels. Using the above-

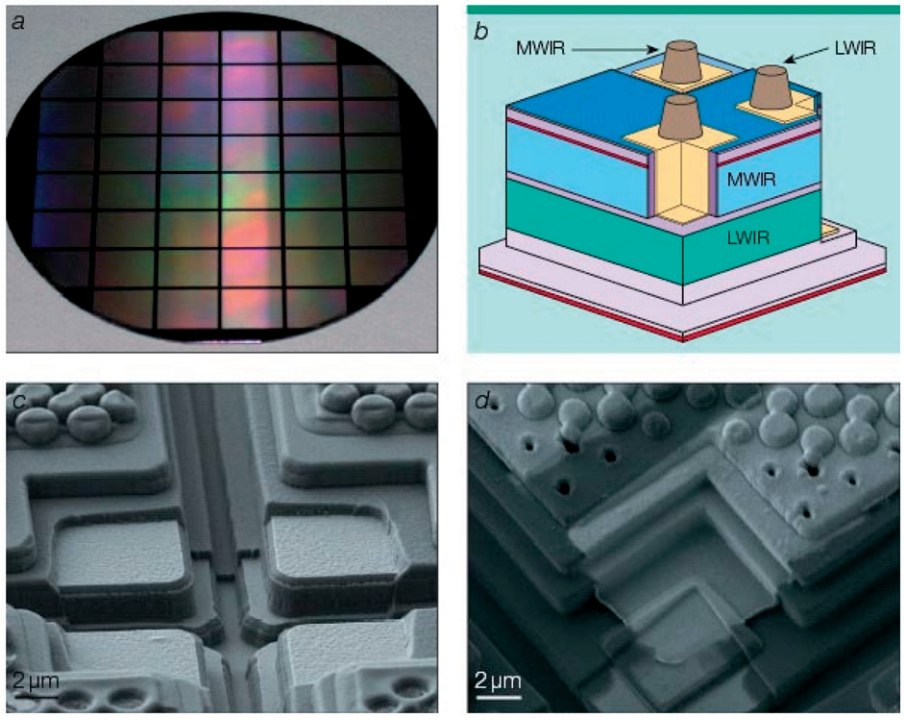

Figure 11. Two-color MWIR/LWIR QWIP FPA: (*a*) 48 FPAs processed on a 4 inch GaAs wafer, (*b*) 3D view of pixel structure, (*c*) electrical connections to the common contact, (*d*) the pixel connections are brought to the top of each pixel using the gold via connections (after [67]). (The color version of this figure is included in the online version of the journal.)

described fabrication process, significant progress has been made towards development of a megapixel dual-band QWIP FPA [53,54,67].

Development of dual-band QWIP FPAs has been undertaken over the last decade. One of the key issues has been the scarcity of appropriate read-out multiplexers. To overcome this problem, JPL has chosen to demonstrate initial dual band concepts with existing multiplexers developed for single-color applications, and use a waveband-interlaced CMOS readout architecture (i.e. odd rows for one color and even rows for the other color). This scheme has the disadvantage that it does not provide a full fill factor for both wavelength bands, resulting in an approximate 50% fill factor for each wavelength band. At present, QWIP FPA with pixel co-llocation and simultaneous operation in MWIR and LWIR are fabricated. Typical operating temperatures for QWIP detectors are in the range of 60 to 80 K. The bias across each QWIP can be adjusted separately, although it is desirable to apply the same bias to both colors.

Thales selected the ISC0208 Indigo ROIC for demonstration of a prototype dual band QWIP camera. Since this read-out is not designed for dual band applications, the QWIP demonstrator cannot be a temporally coherent MWIR/LWIR array. MWIR/LWIR imagery is based on a two stack quantum structure (see Figure 12) and is described in [68]. The processing is the same as the one developed for *in situ* skimming FPAs [69]. One band is read when the second one is integrated, hence the two QWIP biases are modulated between two frames. The QWIP wafers were processed with the 25 μm pitch, 384×288 format of the ISC0208 ROIC. The SEM picture in Figure 12(*b*) illustrates details of the processing.

To cover the MWIR range, a strained-layer InGaAs/AlGaAs material system is used. InGaAs in the MWIR stack produces high in-plane compressive strain, which enhances the responsivity.

Recently, the research group from Jet Propulsion Laboratory has implemented a MWIR/LWIR pixel co-registered simultaneously readable 1024×1024 dual-band device structure that uses only two indium bumps per pixel (Figure 13) compared to three indium bumps per pixel with pixel co-located dual-band devices. In this device structure the detector common (or ground) is shorted to the bottom detector common plane via a metal bridge. Thus, this device structure reduces the number of indium bumps by 30% and has a unique advantage in large format FPAs, since more indium bumps require additional force during the FPA hybridization process. The pitch of the detector array is 30 μm and the actual MWIR and LWIR pixel sizes are $28 \times 28\,\mu m^2$. The estimated *NEDT* based on single pixel data of MWIR and LWIR detectors at 70 K are 22 and 24 mK, respectively. The experimentally

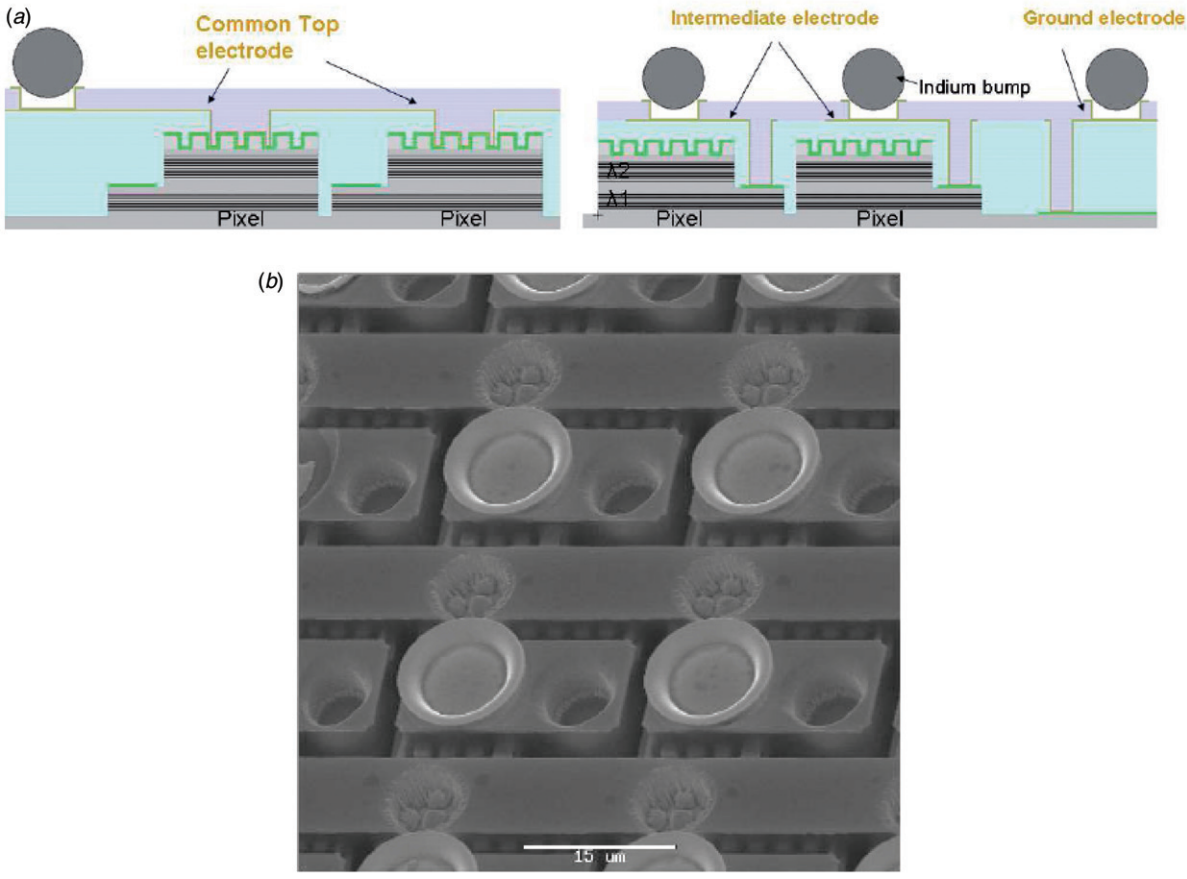

Figure 12. Dual band QWIP array: (*a*) cross-section of two different sections and (*b*) details of a dual band QWIP array with 25 μm pitch (after [64]). (The color version of this figure is included in the online version of the journal.)

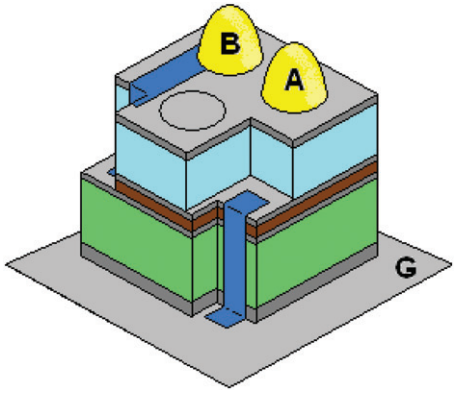

Figure 13. 3D view of dual-band QWIP device structure showing via connects for independent access of MWIR and LWIR devices. The color code is as follows, orange – isolation layer; green – LWIR QWIP; light blue – MWIR QWIP; gray – contact layer; dark blue – metal bridges between MQW regions; yellow – indium bumps (after [55]). (The color version of this figure is included in the online version of the journal.)

measured *NEDT* values were 27 and 40 mK for MWIR and LWIR, respectively.

The potential of QWIP technology is connected with multicolor detection. A four-band hyper spectral 640×512 QWIP array was successfully developed under a joint Goddard–Jet Propulsion Laboratory–Army Research Laboratory project funded by the Earth Science Technology Office of NASA (see Figure 14). The device structure consists of a 15-period stack of 3 to 5 μm QWIP structure, a 25-period stack of 8.5 to 10 μm QWIP structure, a 25-period stack of 10 to 12 μm QWIP structure, and a 30-period stack of 14 to 15.5 μm QWIP structure [52]. The four bands of the QWIP array were defined by a deep trench etch process and the unwanted spectral bands were eliminated by a detector short-circuiting process using gold-coated reflective 2D etched gratings as shown in Figure 14(*a*). The VLWIR QWIP structure has been designed to have bound-to-quasibound intersubband absorption, whereas the other QWIP device structures have been designed to have bound-to-continuum intersubband absorption, since

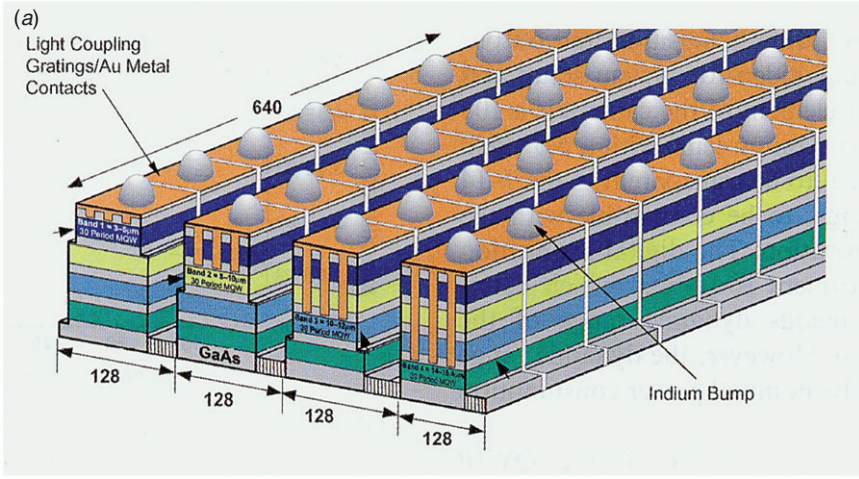

Figure 14. Four-band QWIP device structure: (*a*) layer diagram and the deep groove 2D-periodic grating structure (each pixel represents a 640×128 pixel area of the four-band FPA); (*b*) normalized spectral response (after [52]). (The color version of this figure is included in the online version of the journal.)

the photocurrent and dark current of these devices are small in comparison to those of the VLWIR device.

Recently, a novel four-band IR imaging system with simultaneously readable co-located pixels has been proposed [55]. The FPA is divided into 2×2 sub-pixel areas that function as superpixels marked as Q1, Q2, Q3 and Q4 in Figure 15, each sensitive to one of four specific wavelength bands.

The above results indicate that QWIPs have shown significant progress in recent years, especially in their applications to the multiband imaging problem. It is a niche in which they have an intrinsic advantage due to the comparative ease of growing multiband structures by MBE with very low defect density.

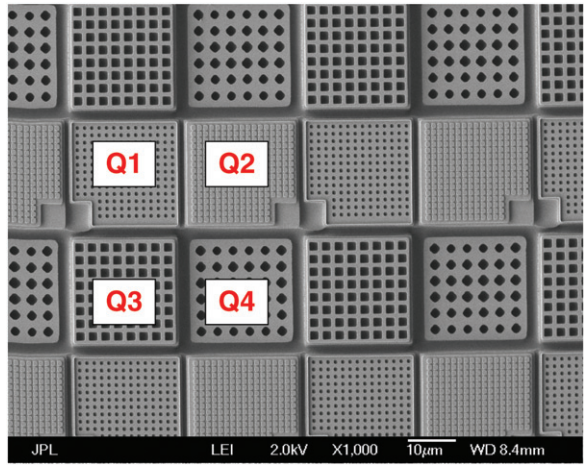

Figure 15. SEM picture of processed four-band array (after [55]). (The color version of this figure is included in the online version of the journal.)

5. Multiband QDIPs

QDIP devices capable of detecting several separate wavelengths can be fabricated by vertical stacking of

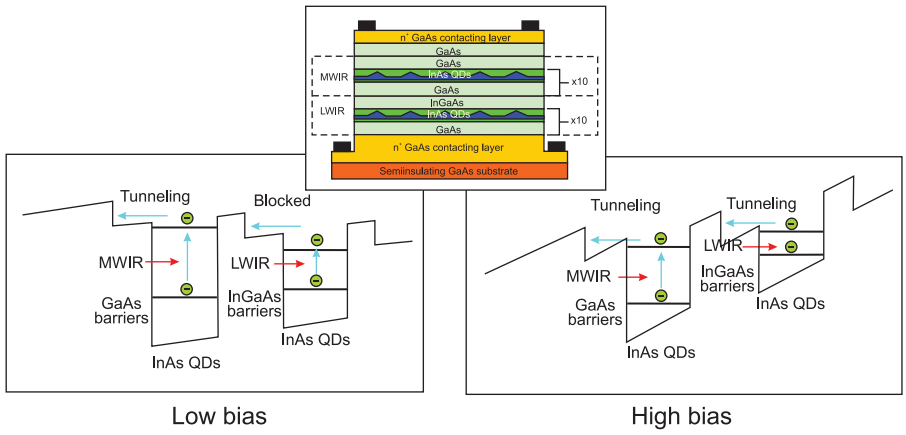

Figure 16. Multispectral QDIP device: simplified band diagram of the structure at different bias levels. In the insert the schematic structure of the device is shown (after [70]). (The color version of this figure is included in the online version of the journal.)

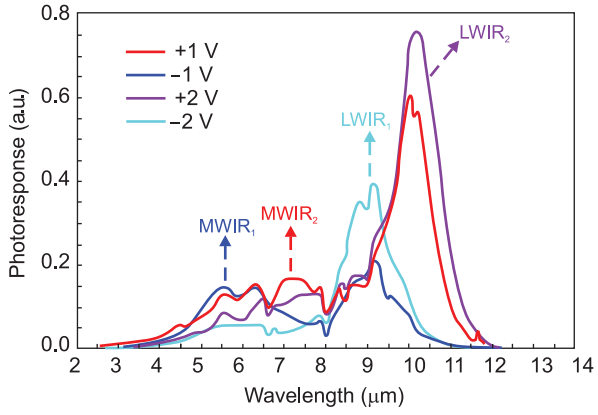

Figure 17. Spectral response from a DWELL detector with response at $V_b = \pm 1$ V and ± 2 V. Note the response in the two MWIR and LWIR bands can be measured using this detector. The relative intensities of the bands can be altered by the applied bias (after [74]). (The color version of this figure is included in the online version of the journal.)

the different QWIP layers during epitaxial growth. The schematic structure is shown in Figure 16. In the case of a structure, described by Lu et al. [70], each QDIP absorption band consists of 10-periods of InAs/InGaAs QD layers sandwiched between the top and bottom electrodes. The bias voltage selection of the detection bands originates from the asymmetric band structure. At low bias voltage, the high energy GaAs barrier blocks the photocurrent generated by LWIR radiation and only responds to the MWIR incidence. Conversely, as the bias voltage increases, the barrier energy decreases, allowing LWIR signals to be detected at different bias voltage levels.

The first two-color quantum dot FPA demonstration was based on a voltage-tunable InAs/InGaAs/GaAs DWELL structure [71,72]. In this type of structure, InAs QDs are placed in an InGaAs well, which in turn is placed in a GaAs matrix.

Figure 17 shows the multicolor response from a DWELL detector. Typically, the MWIR response dominates at low to nominal voltages due to higher escape probability. With increasing voltage, the LWIR and eventually VLWIR responses are enhanced due to the increased tunneling probability of lower states in the DWELL detector. The bias-dependent shift of the spectral response is observed due to the quantum-confined Stark effect. This voltage-control of spectral response can be exploited to realize spectrally smart sensors whose wavelength and bandwidth can be tuned depending on the desired application [73,74].

Recently, Varley et al. [75] have demonstrated a two-color, MWIR/LWIR, 320×256 FPA based on DWELL detectors. Minimum *NEDT* values of 55 mK (MWIR) and 70 mK (LWIR) were measured (see Figure 18).

To develop an increased functionality at the pixel level for next generation FPAs, the concept of an infrared retina has been proposed [74,76]. In this concept, an array can work similarly to the human eye that has a 'single' FPA but multiple cones. Krishna has discussed this concept considering plasmonic tailoring of the resonance or bias dependent dynamic tuning based on the quantum confined Stark effect or incorporation of avalanche gain to achieve embodiments of the infrared retina [76].

6. Conclusions

Third generation infrared imagers are beginning a challenging road to development. For multiband sensors, boosting the sensitivity in order to maximize

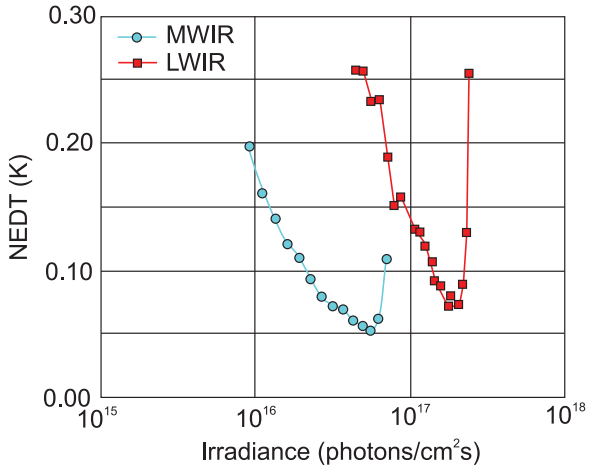

Figure 18. *NEDT* in the MWIR and LWIR bands at 77 K. Irradiance levels for MWIR and LWIR are 3–5 μm (*f*/2) and 8–12 μm (*f*/2.3), respectively (after [75]). (The color version of this figure is included in the online version of the journal.)

the identification range is the primary objective. The goal for dual-band MW/LW IR FPAs are 1920 × 1080 pixels, which due to lower cost should be fabricated on silicon wafers. The challenges to attaining those specifications are material uniformity and defects, heterogeneous integration with silicon and ultra well capacity (on the order of a billion in the LWIR).

It is predicted that HgCdTe technology will continue in the future to expand the envelope of its capabilities because of its excellent properties. Despite serious competition from alternative technologies and slower progress than expected, HgCdTe is unlikely to be seriously challenged for high-performance applications, applications requiring multispectral capability and fast response. However, the nonuniformity is a serious problem in the case of LWIR and VLWIR HgCdTe detectors. For applications that require operation in the LWIR band as well as two-color MWIR/LWIR/VLWIR bands most probably HgCdTe will not be the optimal solution. Type II InAs/GaInSb superlattice structure is a relatively new alternative IR material system and has great potential for LWIR/VLWIR spectral ranges with performance comparable to HgCdTe with the same cutoff wavelength.

Based on the breakthrough of Sb-based type II SLS technology it is obvious that this material system is in a position to provide high thermal resolution for short integration times comparable to HgCdTe. The fact that Sb-based superlattices are processed close to standard III–V technology raises the potential to be more competitive due to lower costs in series production. The potential low cost compared to HgCdTe is that it can leverage investments in lasers and transistors in the Sb-based industry, and has potential commercial market applications in the future.

QDIP detector technology is at a very early stage of development. The bias-dependent spectral diversity of this type of detector can be exploited to realize spectrally smart sensors whose wavelength and bandwidth can be tuned depending on the desired application. Optimization of the QDIP architecture is still an open area. Improving QD uniformity is a key issue in increasing the absorption coefficient and improving the performance.

References

[1] Rogalski, A.; Antoszewski, J.; Faraone, L. *J. Appl. Phys.* **2009,** *105,* 091101.
[2] Reago, D.; Horn, S.; Campbell, J.; Vollmerhausen, R. *Proc. SPIE* **1999,** *3701,* 108–117.
[3] Norton, P.; Campbell, J.; Horn, S.; Reago, D. *Proc. SPIE* **2000,** *4130,* 226–236.
[4] Horn, S.; Norton, P.; Carson, K.; Eden, R.; Clement, R. *Proc. SPIE* **2004,** *5406,* 332–340.
[5] Balcerak, R.; Horn, S. *Proc. SPIE* **2005,** *5783,* 384–391.
[6] Norton, P.R. *Opto-Electron. Rev.* **2006,** *14,* 283–296.
[7] Destefanis, G.; Baylet, J.; Ballet, P.; Castelein, P.; Rothan, F.; Gravrand, O.; Rothman, J.; Chamonal, J.P.; Million, A. *J. Electron. Mater.* **2007,** *36,* 1031–1044.
[8] Smith, E.P.G.; Venzor, G.M.; Petraitis, Y.; Liguori, M.V.; Levy, A.R.; Rabkin, C.K.; Peterson, J.M.; Reddy, M.; Johnson, S.M.; Bangs, J.W. *J. Electron. Mater.* **2007,** *36,* 1045–1051.
[9] Halpert, H.; Musicant, B.I. *Appl. Opt.* **1972,** *11,* 2157–2161.
[10] Rolls, W. *Infrared Phys.* **1977**, *17*, 419–421.
[11] Campbell, J.C.; Dentai, A.G.; Lee, T.P.; Burrus, C.A. *IEEE J. Quantum Electron.* **1980,** *QE-16,* 601–603.
[12] Blazejewski, E.R.; Arias, J.M.; Williams, G.M.; McLevige, W.; Zandian, M.; Pasko, J. *J. Vac. Sci. Technol. B* **1992,** *10,* 1626–1632.
[13] Wilson, J.A.; Patten, E.A.; Chapman, G.R.; Kosai, K.; Baumgratz, B.; Goetz, P.; Tighe, S.; Risser, R.; Herald, R.; Radford, W.A.; Tung, T.; Terre, W.A. *Proc. SPIE* **1994,** *2274,* 117–125.
[14] Rajavel, R.D.; Jamba, D.M.; Jensen, J.E.; Wu, O.K.; Wilson, J.A.; Johnson, J.L.; Patten, E.A.; Kasai, K.; Goetz, P.M.; Johnson, S.M. *J. Electron. Mater.* **1998,** *27,* 747–751.
[15] Smith, E.P.G.; Pham, L.T.; Venzor, G.M.; Norton, E.M.; Newton, M.D.; Goetz, P.M.; Randall, V.K.; Gallagher, A.M.; Pierce, G.K.; Patten, E.A.; Coussa, R.A.; Kosai, K.; Radford, W.A.; Giegerich, L.M.; Edwards, J.M.; Johnson, S.M.; Baur, S.T.; Roth, J.A.; Nosho, B.; De Lyon, T.J.; Jensen, J.E.; Longshore, R.E. *J. Electron. Mater.* **2004,** *33,* 509–516.
[16] Radford, W.A.; Patten, E.A.; King, D.F.; Pierce, G.K.; Vodicka, J.; Goetz, P.; Venzor, G.; Smith, E.P.; Graham, R.; Johnson, S.M.; Roth, J.; Nosho, B.; Jensen, J. *Proc. SPIE* **2005,** *5783,* 331–339.

[17] King, D.F.; Radford, W.A.; Patten, E.A.; Graham, R.W.; McEwan, T.F.; Vodicka, J.G.; Bornfreund, R.F.; Goetz, P.M.; Venzor, G.M.; Johnson, S.M. *Proc. SPIE* **2006,** *6206,* 62060W.

[18] Smith, E.P.G.; Patten, E.A.; Goetz, P.M.; Venzor, G.M.; Roth, J.A.; Nosho, B.Z.; Benson, J.D.; Stoltz, A.J.; Varesi, J.B.; Jensen, J.E.; Johnson, S.M.; Radford, W.A. *J. Electron. Mater.* **2006,** *35,* 1145–1152.

[19] King, D.F.; Graham, J.S.; Kennedy, A.M.; Mullins, R.N.; McQuitty, J.C.; Radford, W.A.; Kostrzewa, T.J.; Patten, E.A.; McEwan, T.F.; Vodicka, J.G.; Wootana, J.J. *Proc. SPIE* **2008,** *6940,* 69402R.

[20] Smith, E.P.G.; Gallagher, A.M.; Kostrzewa, T.J.; Brest, M.L.; Graham, R.W.; Kuzen, C.L.; Hughes, E.T.; McEwan, T.F.; Venzor, G.M.; Patten, E.A.; Radford, W.A. *Proc. SPIE* **2009,** *7298,* 72981Y.

[21] Reine, M.B.; Hairston, A.; O'Dette, P.; Tobin, S.P.; Smith, F.T.J.; Musicant, B.L.; Mitra, P.; Case, F.C. *Proc. SPIE* **1998,** *3379,* 200–212.

[22] Zanatta, J.P.; Ferret, P.; Loyer, R.; Petroz, G.; Cremer, S.; Chamonal, J.P.; Bouchut, P.; Million, A.; Destefanis, G. *Proc. SPIE* **2000,** *4130,* 441–451.

[23] Tribolet, P.; Vuillermet, M.; Destefanis, G. *Proc. SPIE* **2005,** *5964,* 49–60.

[24] Destefanis, G.; Ballet, P.; Baylet, J.; Castelein, P.; Gravrand, O.; Rothman, J.; Rothan, F.; Perrais, G.; Chamonal, J.P.; Million, A.; Tribolet, P.; Terrier, B.; Sanson, E.; Costa, P.; Vial, L. *Proc. SPIE* **2006,** *6206,* 62060R.

[25] Zanatta, J.P.; Badano, G.; Ballet, P.; Largeron, C.; Baylet, J.; Gravrand, O.; Rothman, J.; Castelein, P.; Chamonal, J.P.; Million, A.; Destefanis, G.; Mibord, S.; Brochier, E.; Costa, P. *J. Electron. Mater.* **2006,** *35,* 1231–1236.

[26] Destefanis, G.; Baylet, J.; Ballet, P.; Castelein, P.; Rothan, F.; Gravrand, O.; Rothman, J.; Chamonal, J.P.; Million, A. *J. Electron. Mater.* **2007,** *36,* 1031–1044.

[27] Tribolet, P.; Destefanis, G.; Ballet, P.; Baylet, J.; Gravrand, O.; Rothman, J. *Proc. SPIE* **2008,** *6940,* 69402P.

[28] Giess, J.; Glover, M.A.; Gordon, N.T.; Graham, A.; Haigh, M.K.; Hails, J.E.; Hall, D.J.; Lees, D.J. *Proc. SPIE* **2005,** *5783,* 316–324.

[29] Gordon, N.T.; Abbott, P.; Giess, J.; Graham, A.; Hails, J.E.; Hall, D.J.; Hipwood, L.; Lones, C.L.; Maxey, C.D.; Price, J. *J. Electron. Mater.* **2007,** *36,* 931–936.

[30] Jones, C.L.; Hipwood, L.G.; Price, J.; Shaw, C.J.; Abbott, P.; Maxey, C.D.; Lau, H.W.; Catchpole, R.A.; Ordish, M.; Knowles, P.; Gordon, N.T. *Proc. SPIE* **2007,** *6542,* 654210.

[31] Price, J.P.G.; Jones, C.L.; Hipwood, L.G.; Shaw, C.J.; Abbott, P.; Maxey, C.D.; Lau, H.W.; Fitzmaurice, J.; Catchpole, R.A.; Ordish, M.; Thorne, P.; Weller, H.J.; Mistry, R.C.; Hoade, K.; Bradford, A.; Owton, D.; Knowles, P. *Proc. SPIE* **2008,** *6940,* 69402S.

[32] Kinch, M.A. *Proc. SPIE* **2001,** *4369,* 566–578.

[33] Dreiske, P.D. *Proc. SPIE* **2005,** *5783,* 325–330.

[34] Aqariden, F.; Dreiske, P.D.; Kinch, M.A.; Liao, P.K.; Murphy, T.; Schaake, H.F.; Shafer, T.A.; Shih, H.D.; Teherant, T.H. *J. Electron. Mater.* **2007,** *36,* 900–904.

[35] Tennant, W.E.; Thomas, M.; Kozlowski, L.J.; McLevige, W.V.; Edwall, D.D.; Zandian, M.; Spariosu, K.; Hildebrandt, G.; Gil, V.; Ely, P.; Muzilla, M.; Stoltz, A.; Dinan, J.H. *J. Electron. Mater.* **2001,** *30,* 590–594.

[36] Almeida, L.A.; Thomas, M.; Larsen, W.; Spariosu, K.; Edwall, D.D.; Benson, J.D.; Mason, W.; Stoltz, A.J.; Dinan, J.H. *J. Electron. Mater.* **2002,** *30,* 669–676.

[37] Smith, E.P.G.; Bornfreund, R.E.; Kasai, I.; Pham, L.T.; Patten, E.A.; Peterson, J.M.; Roth, J.A.; Nosho, B.Z.; Lyon, T.J.; Jensen, J.E.; Bangs, J.W.; Johnson, S.M.; Radford, W.A. *Proc. SPIE* **2006,** *6127,* 61271F.

[38] Lockwood, A.H.; Balon, J.R.; Chia, P.S.; Renda, F.J. *Infrared Phys.* **1976,** *16,* 509–514.

[39] Norton, P.R. *Proc. SPIE* **1998,** *3379,* 102–114.

[40] Wei, Y.; Razeghi, M. *Phys. Rev. B* **2004,** *69,* 085316.

[41] Rehm, R.; Walther, M.; Schmitz, J.; Fleißner, J.; Fuchs, F.; Ziegler, J.; Cabanski, W. *Opto-Electron. Rev.* **2006,** *14,* 283–296.

[42] Münzberg, M.; Breiter, R.; Cabanski, W.; Lutz, H.; Wendler, J.; Ziegler, J.; Rehm, R.; Walther, M. *Proc. SPIE* **2006,** *6206,* 620627.

[43] Rehm, R.; Walther, M.; Schmitz, J.; Fleißner, J.; Ziegler, J.; Cabanski, W.; Breiter, R. *Proc. SPIE* **2006,** *6292,* 629404.

[44] Münzberg, M.; Breiter, R.; Cabanski, W.; Hofmann, K.; Lutz, H.; Wendler, J.; Ziegler, J.; Rehm, R.; Walther, M. *Proc. SPIE* **2007,** *6542,* 654207.

[45] Rutz, F.; Rehm, R.; Schmitz, J.; Fleissner, J.; Walther, M.; Scheibner, R.; Ziegler, J. *Proc. SPIE* **2009,** *7298,* 72981R.

[46] Razeghi, M.; Hoffman, D.; Nguyen, B.M.; Delaunay, P.-Y.; Huang, E.K.; Tidrow, M.Z.; Nathan, V. *Proc. IEEE* **2009,** *97,* 1056–1066.

[47] Beck, W.A.; Faska, T.S. *Proc. SPIE* **1996,** *2744,* 193–206.

[48] Sundaram, M.; Wang, S.C. *Proc. SPIE* **2000,** *4028,* 311–317.

[49] Gunapala, S.D.; Bandara, S.V.; Singh, A.; Liu, J.K.; Rafol, S.B.; Luong, E.M.; Mumolo, J.M.; Tran, N.Q.; Vincent, J.D.; Shott, C.A.; Long, J.; LeVan, P.D. *Proc. SPIE* **1999,** *3698,* 687–697.

[50] Gunapala, S.D.; Bandara, S.V.; Singh, A.; Liu, J.K.; Rafol, B.; Luong, E.M.; Mumolo, J.M.; Tran, N.Q.; Ting, D.Z.; Vincent, J.D.; Shott, C.A.; Long, J.; LeVan, P.D. *IEEE Trans. Electron. Devices* **2000,** *47,* 963–971.

[51] Gunapala, S.D.; Bandara, S.V.; Liu, J.K.; Luong, E.M.; Rafol, S.B.; Mumolo, J.M.; Ting, D.Z.; Bock, J.J.; Ressler, M.E.; Werner, M.W.; LeVan, P.D.; Chehayeb, R.; Kukkonen, C.A.; Ley, M.; LeVan, P.; Fauci, M.A. *Opto-Electron. Rev.* **2001,** *8,* 150–163.

[52] Gunapala, S.D.; Bandara, S.V.; Liu, J.K.; Rafol, B.; Mumolo, J.M.; Shott, C.A.; Jones, R.; Woolaway, J.; Fastenau, J.M.; Liu, A.K.; Jhabvala, M.; Choi, K.K. *Infrared Phys. Technol.* **2003,** *44,* 411–425.

[53] Gunapala, S.D.; Bandara, S.V.; Liu, J.K.; Mumolo, J.M.; Hill, C.J.; Rafol, S.B.; Salazar, D.; Woolaway, J.; LeVan, P.D.; Tidrow, M.Z. *Infrared Phys. Technol.* **2007,** *50,* 217–226.

[54] Gunapala, S.D.; Bandara, S.V.; Liu, J.K.; Mumolo, J.M.; Hill, C.J.; Ting, D.Z.; Kurth, E.; Woolaway, J.; LeVan, P.D.; Tidrow, M.Z. *Proc. SPIE* **2008,** *6940,* 69402T.
[55] Soibel, A.; Gunapala, S.D.; Bandara, S.V.; Liu, J.K.; Mumolo, J.M.; Ting, D.Z.; Hill, C.J.; Nguyen, J. *Proc. SPIE* **2009,** *7298,* 729806.
[56] Goldberg, A.; Fischer, T.; Kennerly, J.; Wang, S.; Sundaram, M.; Uppal, P.; Winn, M.; Milne, G.; Stevens, M. *Proc. SPIE* **2000,** *4028,* 276–287.
[57] Goldberger, A.C.; Kennerly, S.W.; Little, J.W.; Pollehn, H.K.; Shafer, T.A.; Mears, C.L.; Schaake, H.F.; Winn, M.; Taylor, M.; Uppal, P.N. *Proc. SPIE* **2001,** *4369,* 532–546.
[58] Choi, K.-K.; Jhabvala, M.D.; Peralta, R.J. *IEEE Electron. Dev. Lett.* **2008,** *29,* 1011–1013.
[59] Jhabvala, M. *Infrared Phys. Technol.* **2001,** *42,* 363–376.
[60] Costard, E.; Bois, Ph.; Marcadet, X.; Nedelcu, A. *Proc. SPIE* **2005,** *5783,* 728–735.
[61] Manissadjian, A.; Gohier, D.; Costard, E.; Nedelcu, A. *Proc. SPIE* **2006,** *6206,* 62060E.
[62] Nedelcu, A.; Costard, E.; Bois, P.; Marcadet, X. *Infrared Phys. Technol.* **2007,** *50,* 227–233.
[63] Perrin, N.; Belhaire, E.; Marquet, P.; Besnard, V.; Costard, E.; Nedelcu, A.; Bois, P.; Craig, R.; Parsons, J.; Johnston, W.; Manissadjian, A.; Guinche, Y. *Proc. SPIE* **2008,** *6940,* 694008.
[64] Robo, J.A.; Costard, E.; Truffer, J.P.; Nedelcu, A.; Marcadet, X.; Bois, P. *Proc. SPIE* **2009,** *7298,* 72980F.
[65] Cabanski, W.; Münzberg, M.; Rode, W.; Wendler, J.; Ziegler, J.; Fleißner, J.; Fuchs, F.; Rehm, P.; Schmitz, J.; Schneider, H.; Walther, M. *Proc. SPIE* **2005,** *5783,* 340–349.
[66] Schneider, H.; Maier, T.; Fleissner, J.; Walther, M.; Koidl, P.; Weimann, G.; Cabanski, W.; Finck, M.; Menger, P.; Rode, W.; Ziegler, J. *Infrared Phys. Technol.* **2005,** *47,* 53–58.
[67] Gunapala, S. *Compd. Semicond.* **2005,** *10,* 25–28.
[68] Castelein, P.; Guellec, F.; Rothan, F.; Martin, S.; Bois, P.; Costard, E.; Huet, O.; Marcadet, X.; Nedelcu, A. *Proc. SPIE* **2005,** *5783,* 804–815.
[69] Bois, P.; Costard, E.; Marcadet, X.; Herniou, E. *Infrared Phys. Technol.* **2001,** *42,* 291–300.
[70] Lu, X.; Vaillancourt, J.; Meisner, M. *Proc. SPIE* **2007,** *6542,* 65420Q.
[71] Krishna, S.; Forman, D.; Annamalai, S.; Dowd, P.; Varangis, P.; Tumolillo, T.; Gray, A.; Zilko, J.; Sun, K.; Liu, M.; Campbell, J.; Carothers, D. *Appl. Phys. Lett.* **2005,** *86,* 193501.
[72] Krishna, S.; Forman, D.; Annamalai, S.; Dowd, P.; Varangis, P.; Tumolillo, T.; Gray, A.; Zilko, J.; Sun, K.; Liu, M.; Campbell, J.; Carothers, D. *Phys. Stat. Sol. (c)* **2006,** *3,* 439–443.
[73] Krishna, S. *J. Phys. D: Appl. Phys.* **2005,** *38,* 2142–2150.
[74] Krishna, S.; Gunapala, S.D.; Bandara, S.V.; Hill, C.; Ting, D.Z. *Proc. IEEE* **2007,** *95,* 1838–1852.
[75] Varley, E.; Lenz, M.; Lee, S.J.; Brown, J.S.; Ramirez, D.A.; Stintz, A.; Krishna, S. *Appl. Phys. Lett.* **2007,** *91,* 081120.
[76] Krishna, S. *J. Phys. D: Appl. Phys.* **2009,** *42,* 234005.